Available online at www.sciencedirect.com
SCIENCE DIRECT
Cement and Concrete Research 35 (2005) 1613–1619
Cement and Concrete Research

Characterisation of mortar morphology in thin sections by digital image processing

Nicoletta Marinoni[a,*], Alessandro Pavese[a,b], Marco Foi[a], Luca Trombino[a,b]

[a]Dipartimento di Scienze della Terra, Università degli Studi di Milano, Via Botticelli 23, 20133 Milano, Italy
[b]Istituto per la Dinamica dei Processi Ambientali, Sede di Milano, Via Mangiagalli 34, 20133 Milano, Italy

Received 25 January 2004; accepted 10 September 2004

Abstract

A digital imaging approach was applied to investigate mortar morphology in thin sections; in particular, the binder/aggregate ratio and the grading curve of five mortar bars were attained by digital image processing (DIP), using the Image Pro Plus 4.1 software package. The imaging procedure employed image segmentation, to extract mortar aggregate, and image filtering, to fix grain boundaries. The results show that digital image processing may be considered as an alternative method to mechanical sieving for the characterisation of mortar morphology, as it appears to be quicker and more accurate than the traditional method. However, digital image processing exhibits limits, which are discussed in the text.

Keywords: Mortar morphology; Thin sections; Digital image processing

1. Introduction

Digital image processing (DIP) is a computerised technique for image analysis. It consists of a sequence of operations that include: (1) the image acquisition, that is the process of capturing a scene and digitising it into a pixel image; (2) the image processing, i.e. the extraction of quantified information from the digitised image by the analysis of the pixel array [1]. DIP has been widely used in several disciplines such as medicine, biology, material science and in industry, too. For instance, it has been employed for quality control in ceramic manufacturing, for diagnosis of cancer in Pathology, for reconstruction of old irrigation networks from satellite image in Archaeology and in many other fields [2,3]. Previous studies have indicated that digital image processing represents a powerful tool for investigating civil engineering materials, as concerns the morphology of cements and clinkers, as well as the characterisation of pore structure and microcracks in cement paste [4–7].

Several authors have attempted to employ DIP technique for defining the shape, sphericity and other morphological features of concrete aggregates [8–10]. On the other hand, a few applications have focused on the concrete characterisation by DIP on thin sections; this is due to the difficulty in distinguishing boundaries between adjacent, colourless grains, textural features, undulating extinction and twin boundaries [11]. At present, the grading curve, as well as the binder to aggregate ratio of concrete aggregates, is usually determined by mechanical sieving. However, such a traditional method is affected by a significant level of uncertainty leading to a lack of information about the geometrical properties of the particles involved [8]. Moreover, reproducibility and quality of the results depend largely on the personal skills of the operator. This provides a motivation for automating the measurement processes, and the digital image processing methods may be considered a reliable way to such a purpose.

* Corresponding author. Tel.: +39 02 50315575; fax: +39 02 50315597.
E-mail addresses: nicoletta.marinoni@unimi.it (N. Marinoni), alessandro.pavese@unimi.it (A. Pavese), luca.trombino@unimi.it (L. Trombino).

0008-8846/$ - see front matter © 2004 Elsevier Ltd. All rights reserved.
doi:10.1016/j.cemconres.2004.09.015

In the present work, a procedure is proposed for the determination of the mortar aggregate/binder ratio and grading curve on the basis of observations performed on thin sections; thus combining DIP methods with standard optical techniques.

2. Experimental

2.1. Sample preparation

Five mortar bars were prepared by mixing Ordinary Portland Cement (OPC) with known contents of water and aggregate. The aggregate was constituted of rock fragments such as quartzites, cherts, mudstone and sandstone associated with minerals (silicates, calcite, sulphurs and oxides).

A mechanical sieving was used to separate the aggregates into five different fractions by means of a pile of six sieves with 4, 2, 1, 0.5, 0.25 and 0.125 mm aperture size. The grain fractions larger than 4 mm and smaller than 0.125 mm were discarded in order to keep the grain size into the most suitable and commonly used range for modern mortar manufacture. Then, the four aggregate fractions were mixed in different volume percentages to reproduce several grain size distributions; one of this grading curve is the *Fuller Curve* (Mortar Bar F; see Fig. 1a), where an appropriate ratio between fine and coarse fractions provides a good fluidity to the cement paste and gives proper load strength to the mortar once hardened [12].

20×30×50 mm mortar prisms were prepared, with aggregates and cement paste equal to 70:30% in volume, respectively; the water to binder ratio was 0.5 by weight.

The mortars were cured at 20 °C and 25% R.H. throughout the day, and subsequently at 50% R.H. during the following 27 days. Once hardened, they were cut perpendicularly to their major axis to obtain eight slices (2

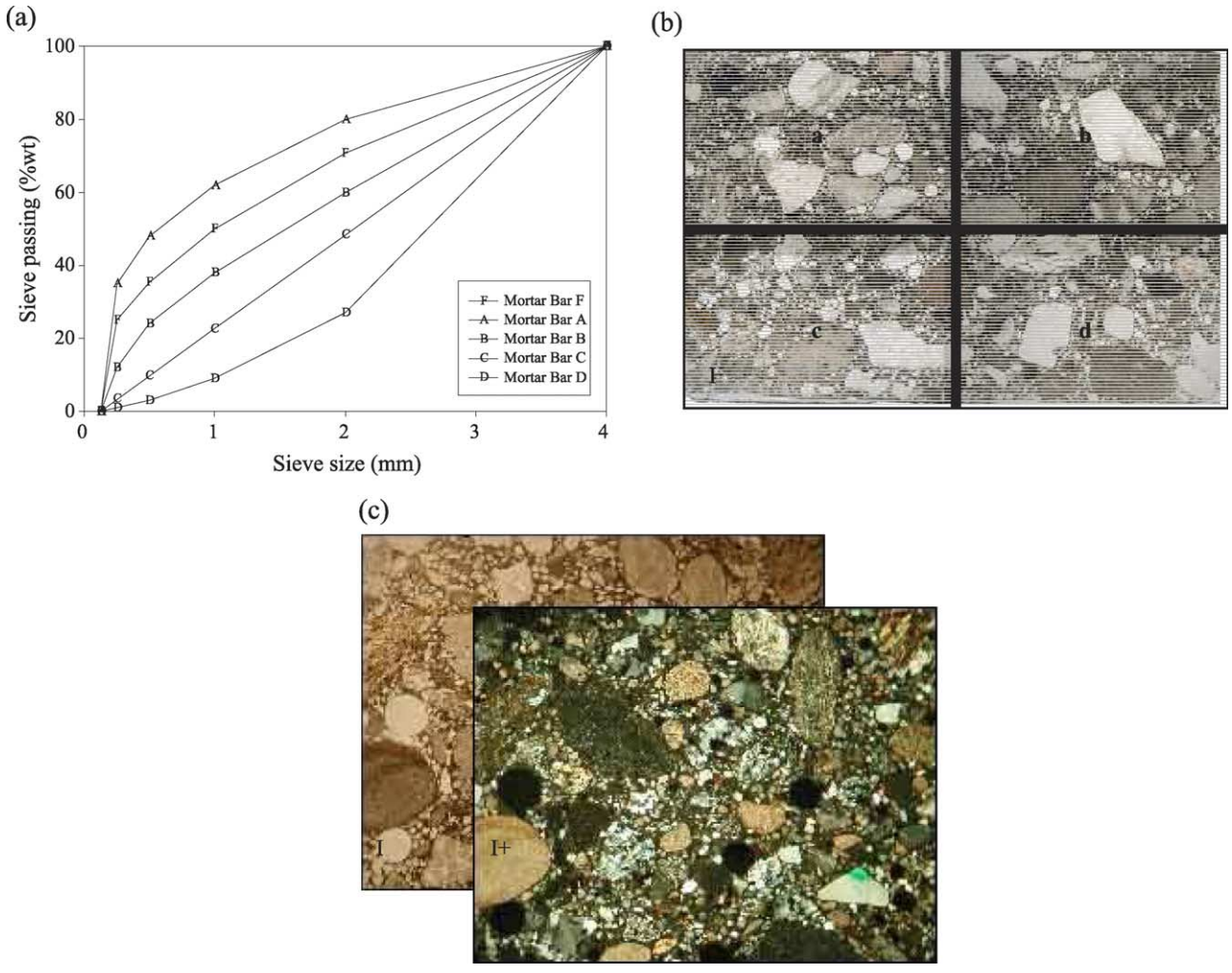

Fig. 1. (a) Aggregate grain size distributions of the experimental mortar bars; (b) four sectors in which each thin section is subdivided ($I\|\|$, 2×); (c) thin section micrograph in crossed ($I+$) and plane-polarised light ($I\|\|$), respectively (3×).

cm in thickness) from which thin section (30 μm in thickness) were carved.

2.2. Digitalisation

Optical observations were performed by a Leica MS5 microscope linked to a 4.1 Gigapixel digital camera Nikon Coolpix 990. Each thin section was investigated at a low magnification (×3), which provided an adequate resolution for the study of the aggregate.

The binder/aggregate ratio was measured on images obtained by dividing each thin section into four sectors (Fig. 1b) of 150 mm^2 area, so that the coarsest aggregates (particles with a grain size of 1–2 mm) had a significant probability to be contained in each sector. The digital images were recorded with a 2045×1536 pixels resolution, where a pixel corresponded approximately to an average linear size of 7 μm, leading to an object resolution of about 40 μm.

For the determination of the grading curve, the low magnification required to divide each thin section into 16 sectors, where a pixel corresponded to 3 μm leading to an object resolution of 15 μm. Such conditions allowed to fix those particles ranging in size from 0.250 to 0.125 mm.

Each sector of the thin section was digitised and stored by a digital camera, connected to the microscope; in particular, two digital images were performed, in crossed ($I+$) and plane-polarised light ($I\|\|$), respectively (Fig. 1c). This procedure allowed to distinguish easily among minerals; for instance, quartz and feldspars are colourless in plane-polarised light, but have distinct interference colours in cross-polarised light.

2.3. Image processing

2.3.1. Binder/aggregate ratio

The imaging procedure to evaluate the mortar binder/aggregate ratio can be summarized in the following steps:

- digitalisation of thin sections (Fig. 2a);
- spatial calibration of the digital images, in order to fix how many pixels correspond to 1 μm in horizontal and vertical direction;
- image thresholding: segmentations were performed to extract single objects, i.e. opaque minerals, air voids, carbonate and silicate aggregates from thin sections, and to produce the corresponding binary images. The main image thresholding steps are summarised as follows:
  (1) detection of air voids and resin borders: the thin section digital images were converted to gray scale images, and an arithmetic operator was used to subtract the cross-polarised light image ($I+$) from the one captured in plane-polarized light ($I\|\|$). Such operation involves one spatial pixel location at a time and each pixel value in the first image is subtracted from its counterpart in the second image [$I\|\|-I+$]; if a pixel intensity lies outside the image intensity scale, it is clipped to the highest/lowest permitted value. The obtained image showed a low brightness, and in the grey level histogram the highest values (the brightest pixels) were associated to the air voids and resin borders. Then, a binary image (A_{voids}) was created where white and black pixels represent the air voids and background, respectively (Fig. 2b);
  (2) detection of opaque minerals: sulphur and oxide minerals were extracted following the same procedure as in the case of the air void segmentation; in particular the in plane-polarised light image was added to the one acquired in cross-polarised light [$I\|\|+I+$]. The obtained image had a grey scale histogram where the darker pixels were associated to the opaque minerals (sulphurs and oxides). The corresponding binary image A_{opaque} (white and black pixels associated to opaque minerals and background, respectively) was created;
  (3) detection of carbonate aggregates: the carbonate segmentation was carried out by a Hue, Saturation and Intensity (HSI) colour model. In particular, the HSI colour components of the carbonate were modelled by analysing the probability density functions of the image pixel values. As pointed out in Fig. 2c the Intensity colour component proved to be the most effective marker to fix the carbonate fraction in the mortar (Fig. 2d); the use of Saturation or Hue colour components gave a certain a degree of uncertainty, which did not allow a reliable discrimination of carbonates from the binder. However, the Intensity is largely affected by the brightness of an image, varying according to the illumination conditions of a thin section. When a thin section receives an inhomogeneous illumination, the Intensity component results in a multilevel histogram, and the HSI colour space is not efficient for the thresholding of an image. As a matter of fact, in the case of inhomogeneous illumination, the operator should isolate the carbonate aggregate manually, treating each aggregate as a homogeneously illuminated object. This segmentation yielded the binary image A_{carb} of the carbonate fraction;
  (4) detection of silicate aggregate: the silicate segmentation was performed by the Red, Green and Blue (RGB) colour model; in the in plane-polarised light image the density function of distribution of the RGB components of the silicate aggregate was estimated according to probabilistic models; the obtained RGB cumulative frequency histogram enabled to extract the silicate fractions from the

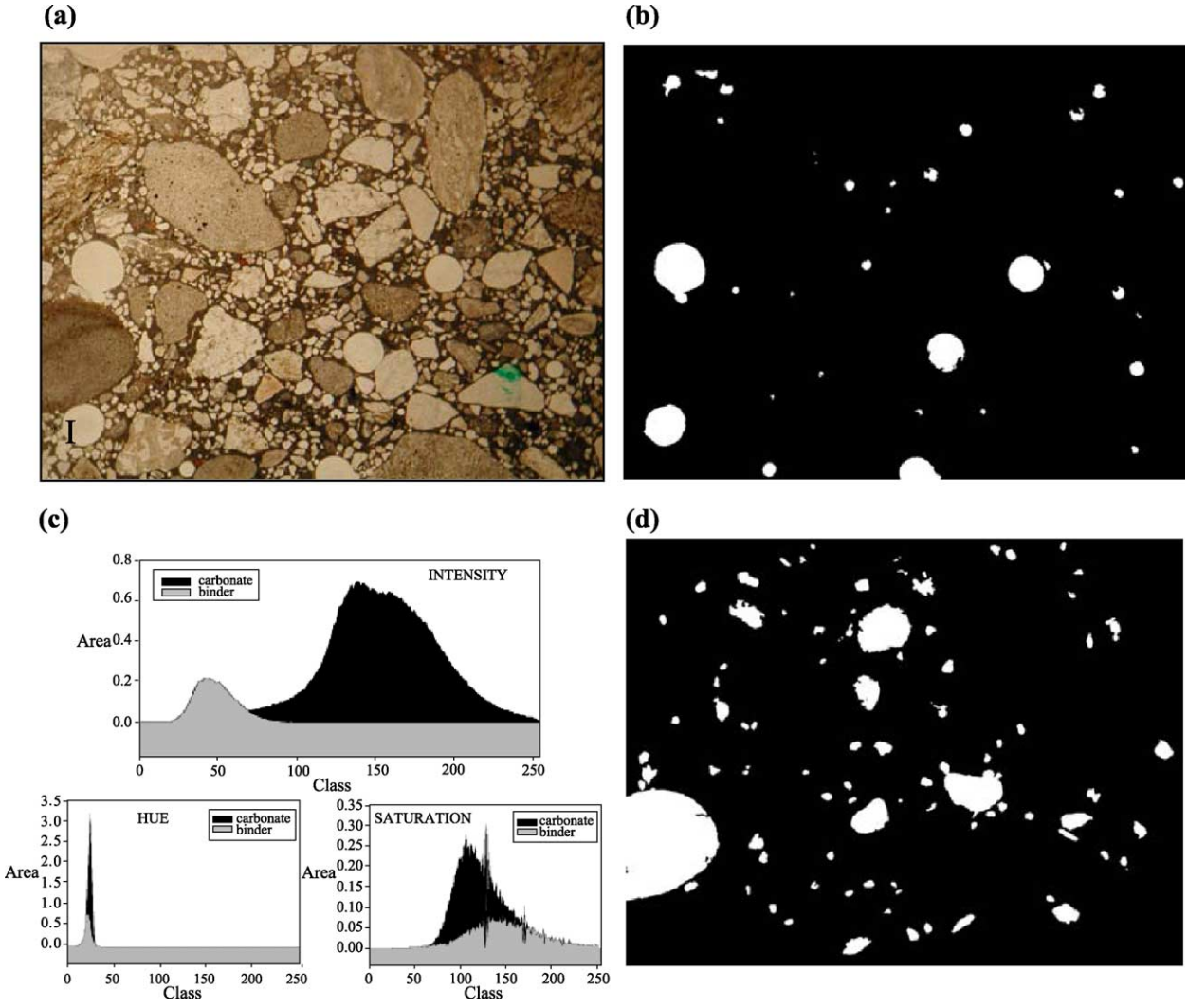

Fig. 2. (a) Example of a digital micrograph used for the image analysis ($I||$, 3×); (b) A_{voids} binary image; (c) cumulative histogram of the HSI components of the carbonate aggregate within a thin section; (d) A_{carb} binary image. See text for details.

whole. Likewise the case of carbonates, the binary image A_{silic} of silicates was generated.

- image measurements and data processing: the binary images from segmentation of aggregate, opaque minerals and air voids were added to a copy of the original in plane-polarised light image $[I||+A_{opaque}+A_{silic}+A_{carb}+A_{voids}]$; in the resulting image the brightest pixels corresponded to air voids, aggregates and opaque minerals, while the darkest ones were associated with the background, i.e. the binder. The grey levels of the pixels of aggregate+opaque+voids were well distinguished from those associated to the background; this allowed to fix the pixels of the binder and the binder to aggregate ratio was achieved.
- statistical analysis: the results were then analysed in terms of their statistical significance (see Section 3).

The overall sequence of operations previously introduced took about 30 min for the binder/aggregate ratio determination.

2.3.2. Mortar grain size distribution

The evaluation of the aggregate grading curve by DIA on thin sections exploited a procedure similar to the one discussed in the case of the binder/aggregate ratio measurement. The binary image of the air voids and resin borders was subtracted from the original in plane-polarised light image, whereas that of the aggregate was added $[I||-A_{voids+}A_{aggregate}]$. In the obtained image, one observed dark objects, i.e. air voids and resin borders, a brownish cement binder and a bright aggregate fraction.

A 3×3 median filter was employed to increase the difference in contrast between the brownish cement and the bright aggregates, while a 3×3 Sobel filter operated to fix the aggregate grain boundaries. The final image

was visually compared with the original in plane-polarised image in order to verify any distortions were not introduced during image processing.

An automatic count/size process measured the areas of the objects, i.e. aggregate particles, which had high pixel intensity values, against a brownish background. The counted objects were then partitioned according to their area into four categories, corresponding to the grain size fractions chosen for the mortar manufacture.

The grain size distribution characterisation took approximately 2 h, as 32 digital images for each thin section were required (16 crossed- and 16 plane-polarised light images).

2.4. Data processing

The average of some physical quantity over a given volume of a mortar can be evaluated according to Eq. (1):

$$\langle \rho \rangle = \frac{1}{V} \int_v \rho(\vec{x}) \mathrm{d}V = \frac{1}{V} \int_z \mathrm{d}z \int_{xy} \rho(xyz) \mathrm{d}x\mathrm{d}y \quad (1)$$

where ρ is a generic observable we are looking at, and V is the volume over which the average is calculated. For instance, in the case of the binder/aggregate ratio, ρ can be 1 if χ belongs to the aggregate and 0 otherwise; this way $\langle \rho \rangle$ measures the volume percentage of aggregate and is readily converted into the binder/aggregate ratio. The equation above can be turned into an approximate form, given by Eq. (2):

$$\langle \rho \rangle = \frac{1}{V} \sum_j \Delta_j \sum_{kl} \rho(klj) \Delta_{kl} \quad (2)$$

where we have replaced the continuous position vector with a discrete triple of indexes klj, which fix a small volume wherein we assume ρ to be constant; and Δ's are in place of the differentials. For a given j, the summation over k and l approximates the two-dimension $\mathrm{d}x\mathrm{d}y$ integration of ρ on a section of the volume V normal to z direction.

If we then assume $\Delta_j = L_z/N_z$, $\Delta_{kl} = S/N_{xy}$ and $V = S^* L_z$, where L_z=length of a bar along z and S=section of a bar normally to z, Eq. (2) turns into Eq. (3):

$$\langle \rho \rangle = \frac{1}{N_z} \sum_j \frac{1}{N_{xy}} \sum_{kl} \rho(klj) \quad (3)$$

The precision of the approximation Eq. (3) depends on (i) the precision in carrying out the two-dimensional integration (summation over k and l) and on (ii) the number of "slices" one uses to model the summation along z (summation over j). While point (i) is a function of our ability to treat and process images, point (ii) is related to how many thin sections we use for studying a given mortar bar.

3. Results and discussion

3.1. Binder/aggregate ratio

The digital image analysis on thin sections provided the area of the aggregate fraction, while the binder fraction was determined as the difference between the total area of the digital image and the aggregate+voids area (for details see Section 2.3). For the sake of brevity the results hereafter introduced refer only to the aggregate fraction, in terms of percentage of aggregate area per image.

As a preliminary test, eight thin sections of the Mortar Bar F were investigated with the aim of evaluating the minimum number of sections required to perform the summation in (Eq. (3)) over j maintaining a relatively low variance. In Fig. 3, the 98% confidence intervals for the averages of the aggregate percentage are plotted as a function of the number of thin sections used. With respect to the case of three thin sections, we observe that the increasing of the thin section number does not provide a significant enhancement in the estimated aggregate percentage. This suggested us to restrict our sampling to three thin sections for each mortar bar, carved at the two ends and in the middle of a bar.

The aggregate percentage for each thin section (Table 1) was determined as the average of the values of the four sectors in which every thin section was partitioned. In turn, the aggregate of every sector is the mean of three independent measurements (standard deviation of ±2%), carried out sequentially. The aggregate percentage value for sector ranges from 62% to 77%, and is reflective of a degree of inhomogeneity of the aggregate distribution within thin sections (Table 1).

The aggregate percentage of each mortar bar, calculated as the arithmetic average of three thin sections, show values from 67% to 74%, with an uncertainty estimated according

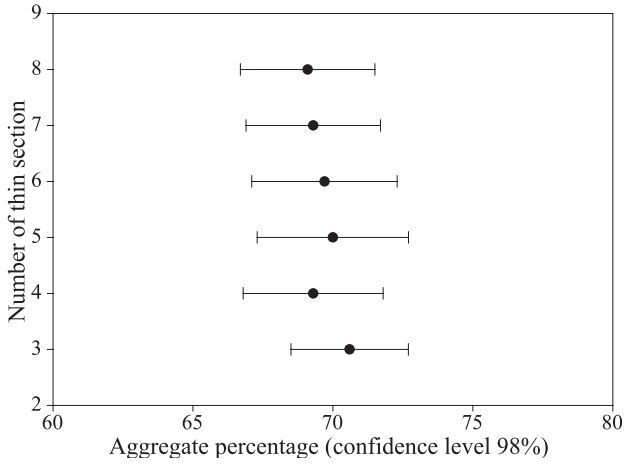

Fig. 3. Confidence intervals of 98% for the aggregate percentage in Mortar Bar F determined by image processing plotted as a function of the number of analysed thin sections (the middle value on the bar is the sample mean and the outer limits depend on the standard deviation).

Table 1
Average content of aggregate percentage, in terms of area, and of binder/aggregate ratio determined by imaging

Mortar Bar	Thin section	% Aggregate						Binder/ aggregate
		Sector				Aver. value[a]	Aver. value[b]	
		a	b	c	d			
A	A1	77	75	76	73	75±1.5	67±1.6	0.49
	A2	72	62	62	63	65±4.2		
	A3	60	63	61	64	62±1.6		
B	B1	69	78	79	81	77±4.6	74±1.7	0.35
	B2	70	71	66	68	69±1.9		
	B3	77	78	75	79	77±1.5		
C	C1	79	74	76	69	75±3.7	72±2.3	0.39
	C2	74	69	67	64	69±3.7		
	C3	79	71	67	69	72±4.6		
D	D1	94	69	70	70	76±10.5	72±4.1	0.39
	D2	64	71	72	60	67±4.9		
	D3	80	70	74	72	74±3.7		
F	F1	72	69	64	69	69±2.9	70±2.1	0.43
	F2	66	71	68	75	70±3.4		
	F3	77	70	71	65	71±4.3		

[a] Refers to the average aggregate percentage of each thin section.
[b] Refers to the average aggregate percentage of each mortar bar.

to the Law of Propagation of Errors [13] always smaller than ±5%. In the last column of the Table 1 the binder/aggregate ratio obtained by digital image analysis on thin sections is reported.

A general overestimation of the aggregate (column Aver. value[b] of Table 1), except for Mortar Bar A, is apparent; note however that the agreement with the actual value is within 3σ. We are inclined to believe that the segmentation is the main source of error as it is based on a simple image thresholding in which the operator interactively chooses the threshold levels of the image to isolate the aggregate fraction against the binder. It is likely that some pixels belonging to the background mingle with the aggregate leading to a larger estimation of the aggregate than the actual value.

As concerns Mortar Bar A, the underestimation in measuring the aggregate percentage of Mortar Bar A is presumably due to the high percentage of the smallest aggregate fraction (35% weight percentage) that mingles with the binder during the image processing. This may be a consequence of a low optical contrast between the smallest aggregate particles and the binder, leading to a confusion of aggregate particles with the background and resulting in an overestimation of the binder against the aggregate percentage.

3.2. Mortar grain size distribution

Before comparing the grain size curve obtained by digital image processing on thin sections with the experimental one, the area fraction of the aggregate particles needs be transformed into a representation of volume or weight percentage. Several studies attempted to define a simple method to convert the particle area measured by DIP to mass fraction [10,14–16]. In the present research we may assume that the aggregate particles in image are projections of spherical objects. This rough approximation is however reasonable given that (i) the minerals of the aggregate do not exhibit systematic preferred orientation, (ii) their shapes, in terms of projection, show a degree of roundness. Each area value was converted into the area of a circle, and the corresponding radius calculated. This allowed to transform a 2D-representation of the material into a 3D-representation.

In Fig. 4, the grain size curve from image processing and the experimental one are compared, showing an excellent agreement. An underestimation occurs for fractions smaller than 2 mm, probably due to fact that spheres do not provide an appropriate model for small

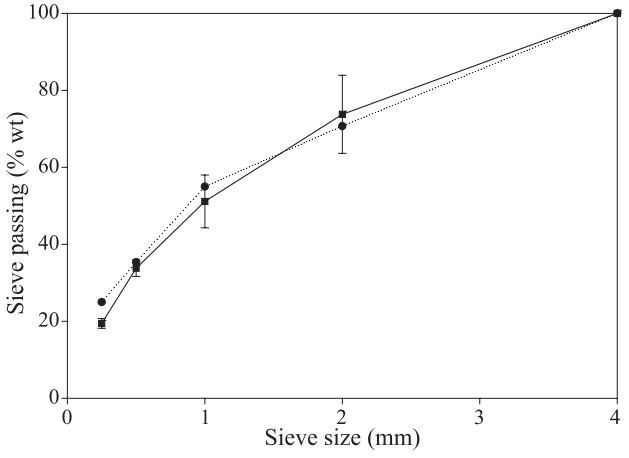

Fig. 4. Comparison between the experimental grading curve and that from digital image analysis. Symbols: ● and ■ refer to the experimental and to the imaging curve, respectively (the middle value on the bar is the sample mean and the outer limits depend on the standard deviation).

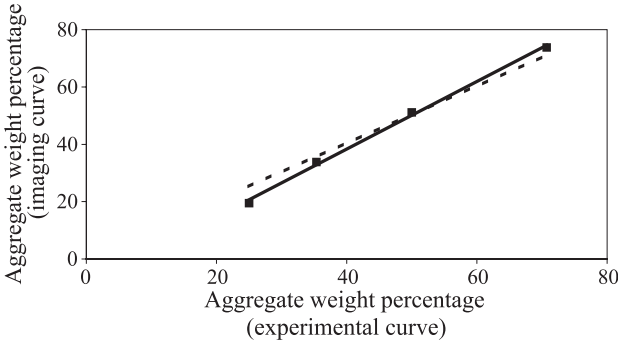

Fig. 5. The size class frequencies from imaging plotted as a function of the size class frequencies of experimental Mortar Bar F. The linear regression (solid line) is compared with equation $y=mx$ (dotted line), corresponding to the ideal case.

particles, which are elongated and/or flanky with rougher surfaces than large particles. The overestimation of the coarse size fraction is still under study, but it is presumably ascribable to the large number of sectors into which each thin section was partitioned causing the largest grains cut over adjacent sectors to fall into incorrect granulometric classes.

In Fig. 5, the size class frequencies from experiments versus those from imaging are shown. A linear regression ($y=mx$; $m=1.0087$) is compared with $y=x$, representing the ideal case in absence of any kind of error in processing images. The modest deviation from 1 of the slope of the obtained correlation is mainly due to the contribution of the smallest size grains related to the low aggregate-binder optical contrast, as mentioned above; this suggests that more effort is to be addressed to improve the treatment of small particles.

4. Conclusion

The application of image analysis on mortars was performed for determining the binder/aggregate ratio and the grading curve, on the basis of observations on thin sections.

Five mortar bars were prepared with known contents of aggregate, cement and water; once hardened, several thin sections were produced and successively investigated by DIP.

The digital image processing employed thresholding (in terms of both grey tone and HSI/RGB colour model) to determine the aggregate, and image filtering to fix the grain boundaries.

The binder/aggregate ratio was evaluated on three thin sections for each mortar, with values ranging from 0.35 to 0.49 (actual value: 0.43). The grading curve extracted from images showed an underestimation of the aggregate smallest particles (deviation from actual value $\approx \pm 6\%$).

These results suggest that the imaging treatment may be an effective alternative to the traditional mechanical sieving. Further investigations are in progress with the aim of determining the mortar morphology by a fully automatic procedure. In particular, a thresholding algorithm, based on statistical inference rather than on visual histogram inspection depending arbitrarily on users, is under study.

References

[1] A.R. Weeks, Fundamentals of Electronic Image Processing, IEEE Press, New York, 1998.
[2] J.L. Chermant, Automatic Image Analysis Today, in: J.L. Chermant (Eds), Microscopy Microanalysis Microstructure Vol. 7 n. 5/6, 20th Anniversary of the French Section of the International Society for Stereology, Les Editions de Physique, France, 1996, pp. 279–288.
[3] P. Campadelli, C. Gangai, F. Pasquale, Automated morphometric analysis in peripheral neuropathies, Comput. Biol. Med. 29 (2) (1999) 147–156.
[4] J.L. Chermant, L. Chermant, M. Coster, A.S. Dequiedt, C. Redon, Some fields of applications of automatic image analysis in civil engineering, Cem. Concr. Compos. 23 (2–3) (2001) 157–169.
[5] M. Coster, J.L. Chermant, Image analysis and mathematical morphology for civil engineering materials, Cem. Concr. Compos. 23 (2–3) (2001) 133–151.
[6] A. Ammouche, D. Breysse, H. Hornain, O. Didry, J. Marchand, A new image analysis technique for the quantitative assessment of microcracks in cement-based materials, Cem. Concr. Res. 30 (1) (2000) 25–35.
[7] P. Navi, P. Pignat, Three-dimensional characterisation of pore structure of a simulated cement paste, Cem. Concr. Res. 29 (4) (1999) 507–514.
[8] C.F. Mora, A.K.H. Kwan, Sphericity, shape factor, and convexity measurement of coarse aggregate for concrete using digital image processing, Cem. Concr. Res. 30 (3) (2000) 351–358.
[9] A.K.H. Kwan, C.F. Mora, H.C. Chan, Particle shape analysis of coarse aggregate using digital image processing, Cem. Concr. Res. 29 (9) (1999) 1403–1410.
[10] C.F. Mora, A.K.H. Kwan, H.C. Chan, Particle size distribution of coarse aggregate using digital image processing, Cem. Concr. Res. 28 (6) (1998) 921–932.
[11] F. Fueten, A computer-controlled rotating polarizer stage for the petrographic microscope, Comput. Geol. 23 (2) (1997) 203–208.
[12] V.A. Rossetti, Il calcestruzzo: materiali e tecnologia, McGraw-Hill Libri, Milano, 1999.
[13] B.R. Martin, Statistics for physicists, Academic Press, London, 1971.
[14] M.D. Higgins, Measurement of crystal size distributions, Am. Mineral. 85 (9) (2000) 1105–1116.
[15] T.D. Peterson, A refined technique for measuring crystal size distributions in thin section, Contrib. Mineral. Petrol. 124 (3–4) (1996) 395–405.
[16] D.L. Sahagian, A.A. Proussevitch, 3D particle size distributions from 2D observations: stereology for natural applications, J. Volcanol. Geotherm. Res. 84 (3–4) (1998) 173–196.